



Production of starch aerogel in form of monoliths and microparticles

Victor Baudron¹ · Martha Taboada² · Pavel Gurikov¹ · Irina Smirnova¹ · Steve Whitehouse³

Received: 13 June 2019 / Revised: 18 December 2019 / Accepted: 12 February 2020 / Published online: 16 March 2020
© The Author(s) 2020

Abstract

Pea and amylo maize starches were used to produce aerogel in form of monoliths and microparticles. The formation of starch gel was investigated, and we showed that each starch needed a different pasting temperature for its complete dissolution. The gelation kinetics was investigated with oscillatory rheometry for both systems as a function of the starch concentration. The gelation and retrogradation temperature of the starch gel were varied and its impact on the final aerogel evaluated. The emulsion gelation was carried out batch wise in a stirred vessel with different impeller geometries, concentrations of surfactant (Span80 and PGPR) and stirring rates. A particle size prediction approach based on idealized flow (Couette, 2D hyperbolic and turbulent) during the emulsification was proposed. A semi-continuous set-up for the emulsion gelation was developed in which the emulsification occurs in a single pass through a colloid mill and the gelation is triggered in-line with a counter-current heat exchanger.

Keywords Starch · Pea · Amylo maize · Pasting · Gelation · Rheometry · Aerogel · Emulsion

Abbreviations

Variables

Ca	[-]	Capillary number
C ₁	[-]	Parameter in de Bruijn fitting for critical capillary number
C ₂	[-]	Parameter in de Bruijn fitting for critical capillary number
Ca _{crit}	[-]	Critical capillary number
D	[m]	Diameter of the impeller or of the colloid mill rotor
d	[m]	Diameter of the droplet
d _{max}	[m]	Largest stable droplet in emulsion
d _T	[m]	Vessel diameter
h _{em}	[m]	Emulsion height in vessel
h _I	[m]	Impeller height
h _T	[m]	Vessel height

K	[Pa.s]	Parameter of the power law model
n	[-]	Parameter of the power law model
N	[min ⁻¹]	Rotational speed in RPM
V _{oil}	[m ³]	Volume of the oil phase
V _{trigger}	[m ³]	Volume of trigger phase
W	[m]	Impeller width
w _{baffle}	[m]	Baffle width

Greek letters

α	[-]	Parameter in de Bruijn fitting for critical capillary number
λ	[-]	Viscosity ratio
λ _{app}	[-]	Apparent viscosity ratio
λ _{max}	[-]	Parameter in de Bruijn fitting for critical capillary number
$\dot{\gamma}$	[s ⁻¹]	Shear rate
$\bar{\gamma}$	[s ⁻¹]	Average shear rate
γ _{max}	[s ⁻¹]	Maximal shear rate
μ	[Pa.s]	Dynamic viscosity
ρ	[kg.m ³]	density
ω	[rad.s ⁻¹]	Rotational speed of the impeller or rotor

✉ Victor Baudron
victor.baudron@tuhh.de

¹ Institute of Thermal Separation Processes, Hamburg University of Technology (TUHH), 22073 Hamburg, Germany

² Institute of Food Process Engineering (LVT), Karlsruhe Institute of Technology (KIT), 76131 Karlsruhe, Germany

³ Nestlé Product Technology Centre York, Haxby Road, PO Box 204, York YO91 1XY, UK

Abbreviations

BET	Brunauer–Emmett–Teller
CMC	Critical micellar concentration
HE	Heat Exchanger

IFT	Interfacial tension
RPM	Rotation per minute
RSM	Rotor stator machine
SEM	Scanning electron microscope

Introduction

Aerogels are mesoporous low density open porous materials with large specific surface area and high specific pore volume. Such properties give them a wide range of potential applications, from carrier material to superinsulation. Aerogel production usually starts with the formation of a gel in water or in an organic solvent. Polysaccharide gels are usually formed in water, which have to be exchanged with an organic solvent to allow for the supercritical drying. During the drying, carbon dioxide and organic solvent form a single supercritical phase that can be removed from the gel while preserving its pore structure.

A wide variety of known gel forming systems gives rise to aerogels with diverse chemical compositions such as inorganic oxides, polysaccharides and synthetic polymers. When gelled in a mould, aerogels adopt its shape. Many examples of monolithic aerogels prepared from synthetic polymers [1–4], cellulose [5–7], pectin [8–10] and alginate [11–13] can be found in the literature.

Starch, being a widely abundant native biopolymer, has attracted attention of the aerogel research: Mehling et al. [14], Marco et al. [15], Ubeyitogullari and Ciftci [16], De Marco and Reverchon [17] and Goimil et al. [18] produced starch aerogel with specific surface areas between 60 and 100 m²/g. Higher values between 220 and 254 m²/g have been reported by Garcia-Gonzalez et al. [19] and Druel et al. [20]. Kenar et al. reached up to 362 m²/g by forming starch-sodium palmitate complexes [21].

Prior research therefore shows that a significant fraction of the overall porosity can be preserved upon conversion into aerogels. Although there is a broad-spectrum of available shaping techniques [22] [23] for gelling systems, such as spraying and jet cutting, little attention has so far been paid to shaping starch aerogels, especially to the production of regular spherical microparticles.

As we reviewed in the work [23], gel microparticles can be obtained via so called emulsion gelation (Fig. 1). In this process, a gelling solution is dispersed in an immiscible oil, and the droplet size is tuned by varying the stirring rate, the emulsifier concentration and other parameters. Once the droplets reach the proper dimensions, the gelation is triggered either by a chemical impact, such as addition of a chemical gelation trigger (e.g. calcium chloride solution for the alginate system [24]), or by a physical impact such as heating (e.g. for proteins [25]) or cooling (e.g. for starch [19]). The gel (micro) particles can then be separated from the oil phase and further processed into aerogel in the same way as their monolithic counterparts.

Particle size and shape of the resulting aerogels are primarily determined by processes in the emulsion, and thus a rational understanding of the process and subsequent scale-up should begin with a closer look at the emulsification step.

Despite the fact that emulsion gelation has been used at lab scale with several polysaccharides such as pectin [26], alginate [26, 27] and starch [19, 26] and also with synthetic polymers [28, 29] and inorganic systems such as silica [30], only batch processes have been reported either with standard impeller or with batch rotor-stator machines. This led Ching et al. [22] to a conclusion that throughput of the emulsion gelation in its batch implementation is strongly limited. To this end, a continuous emulsion gelation could potentially overcome this problem, but such a process has never been reported for the starch system, to the best of our knowledge.

In the present work, we aim to fill the abovementioned gaps by elucidating mechanisms involved into particle formation in the emulsion gelation in order to pave the way to a continuous production of gel and aerogel starch microparticles.

Material and methods

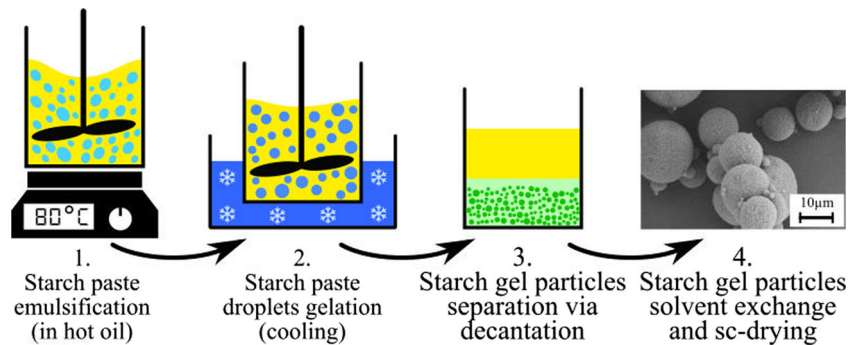
Chemicals

Amylomaize (*High Amylose Corn Starch AMYLO N-460*) and pea (*Pea Native Starch N-735*) starches, with an amylose content of respectively 66 wt.% and 45 wt.% (information provided by furnisher), were kindly provided by Roquette Frere® (Lestrem, France). High- and low-viscosity mineral oil (Carl Roth GmbH) and rapeseed oil (Henry Lamotte) were used to prepare emulsions. Their densities at 20 °C are respectively 880, 850 and 920 kg/m³, and their viscosities were measured at different temperatures and reported in the results part. Sorbitan monooleate, referred as to Span80 (Merck KGaA), and polyglycerol polyricinoleate, referred as to PGPR (PGPR-4150 from Palsgaard), were used as surfactant. Their molecular weights are respectively 428 and 520 g/mol. For the separation and solvent exchange, ethanol solutions were prepared from denatured ethanol (99.8 wt.%) purchased from Carl Roth GmbH.

Pasting

To prepare the starch paste, starch was suspended in cold water in the proportion needed to reach the desired mass fraction. The suspension was then poured into the 200-mL PTFE insert of the pasting autoclave together with a stirring fish. Once the autoclave sealed, the electrical heating was turned on and the temperature increased. The heating duration until the desired temperature varied between 30 and 40 min depending on the desired pasting temperature (ranging between 130 and 140 °C). The temperature was then hold for 20 min

Fig. 1 General scheme of the emulsion gelation method for the starch system



before actively cooling the suspension to 90 °C before opening the autoclave to avoid boiling and water loss.

Gelation investigation with small oscillatory rheology

A rotational rheometer (Malvern Kinexus Pro+) was used for the viscosity measurements and for the investigation of the starch gelation with small oscillation experiments. The viscosity measurements were done with a stainless steel cone and plate geometry (60-mm diameter – 1° angle) and a gap of 0.04 mm. To minimize evaporation of water, a solvent trap was used, and paraffin oil was applied to the edge to avoid sample drying during the measurement. Before depositing the freshly pasted starch (~ 85 °C), the cone and plate were preheated to 80 °C. The oscillatory experiments were done with a plate-plate geometry (20 mm diameter) and a gap of 0.8 mm. The solvent trap and paraffin oil were also used to minimize the water evaporation during the experiment.

Emulsification

Batch emulsifications were carried out in a stirred vessel ($d_T = 66$ mm) equipped with four baffles ($w_{baffle} = 9$ mm). Two impellers were compared, a flat blade turbine (FBT) with diameter $D = 35$ mm and height $h_I = 10$ mm and a 45° pitched blade turbine (PBT) with diameter $D = 38$ mm and height $h_I = 9$ mm, both of them equipped with four blades. The impeller was placed at $3d_I$ from the bottom of the vessel, and the fluid level was $h_{em} = d_T$, producing an emulsification volume of 200 mL. The phase ratio $\Phi = V_{disp}/V_{tot}$ was maintained to 20 v%. After stirring for 10 min, a 1-mL sample was taken for analysis and cooled rapidly to 3 °C to induce a quick gelation of the emulsion droplets so that the particle size distribution of the gel microparticles represented the droplet size distribution in the emulsion.

Semi-continuous emulsifications were carried out with a colloid mill (MagicLab IKA Germany) which rotor had an upper diameter of 22.8 mm and lower diameter of 31.9 mm. Two set-ups were used with the emulsification device as shown in Figs. 2 and 3. With the first one, a coarse emulsion was produced in a jacketed vessel at 80 °C with the PBT at 400 RPM for 5 min and then processed in a one pass through the

colloid mill operated at various rotational speeds and gap widths. A 1-mL sample was cooled down rapidly to 3 °C for analysis and the rest cooled down in a cooling bath.

The second semi-continuous set-up (Fig. 3) consists of a 2-L pasting autoclave equipped with mechanical stirring and a thermostated oil vessel. Once the pasting was finished, the temperature of the starch melt was brought down to the processing temperature, and pressurized air was used to push the starch paste and the oil to the colloid mill. The flow rate could be controlled with the air pressure and by adjusting the valves V1 and V2 that also allowed to control the phase ratio.

With this set-up, a coaxial coil heat exchanger (Table 1) was used to cool down the emulsion and trigger the gelation of the starch paste droplets. It was operated in counter-current mode with cooling water temperature between 17 and 19 °C. The three-way valve V3 was used to take samples before the heat exchanger, which were cooled rapidly and analysed for comparison.

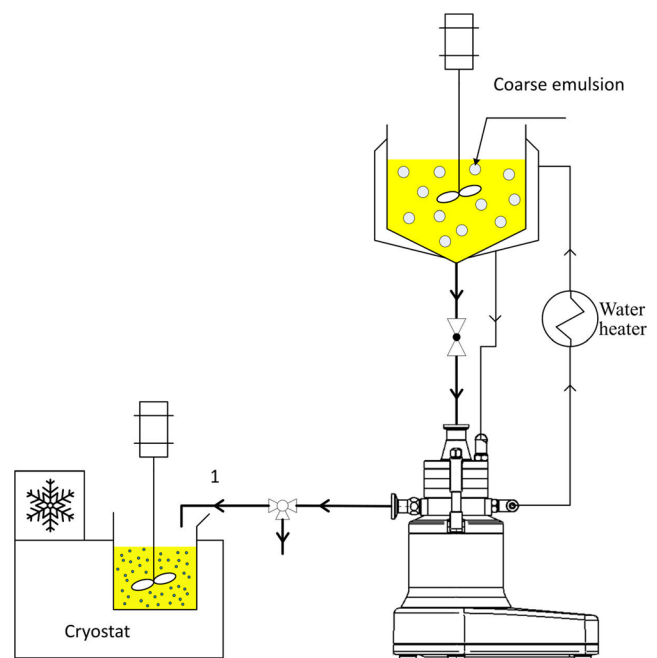
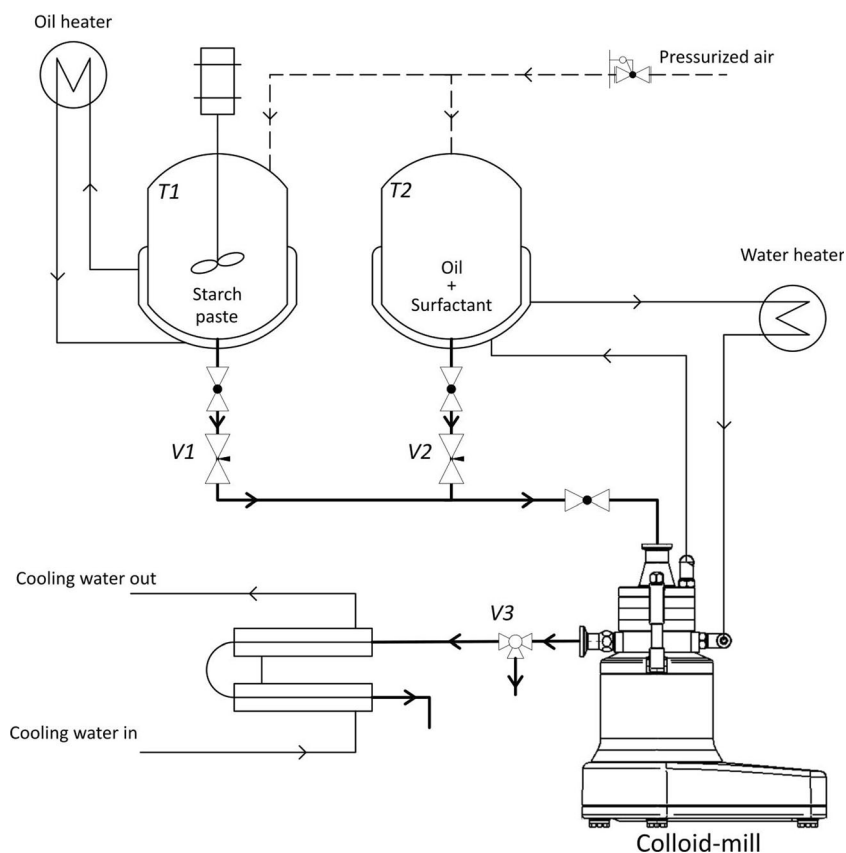


Fig. 2 Semi-continuous set-up: The coarse emulsion is prepared in a stirred vessel before being processed by the colloid mill

Fig. 3 Semi-continuous set-up for the production of starch gel microparticles using an in-line colloid mill as the emulsification device



Particle size distribution measurement

The droplet size distribution of the emulsion was measured by analysing micrographs taken with ten-time magnification objective. Pictures were taken and each droplet/particle was counted one by one with an image analysis program written in Python. Several nonoverlapping pictures were analysed so that more than 1000 different droplets were counted per analysis. Each experiment is repeated twice, and the error bars on the droplet and particle size reported in the graphs correspond to the standard deviation of the two repetitions. The $d_{v,90}$, the 90th percentile of the volume distribution (diameter for which 90% of the total droplet volume is contained in the droplets of diameter $d \leq d_{v,90}$), was taken as the experimental value for the largest stable drop in emulsion similarly to the work by Vankova et al. [31].

Separation, solvent exchange and supercritical drying

To separate the gel microparticles from the oil, a heavier aqueous phase (water or 30 wt.% ethanol) is added. The gel particles being denser than the oil and the aqueous phase, sediment at the bottom of the vessel, can be withdrawn with the aqueous phase.

Subsequently the solvent exchange was done by letting the particles sediment at the bottom of the aqueous phase, removing the supernatant and adding fresh pure ethanol. After gently stirring for 10 min, the cycle was repeated until the ethanol

concentration in the bulk phase reached the desired concentration for drying (> 95%). The solvent exchange of the starch gel monoliths was done in a similar manner, but the system was let to equilibrate overnight before changing the ethanol.

For the supercritical drying, the particles were packed in filter paper and introduced in the supercritical drying autoclave (250 mL, with electrical heating controlling), preheated to 60 °C. The drying was then performed at 120 bar with a continuous flow of CO₂ at 60 °C (~20 g/min) for 3 h.

Results and discussion

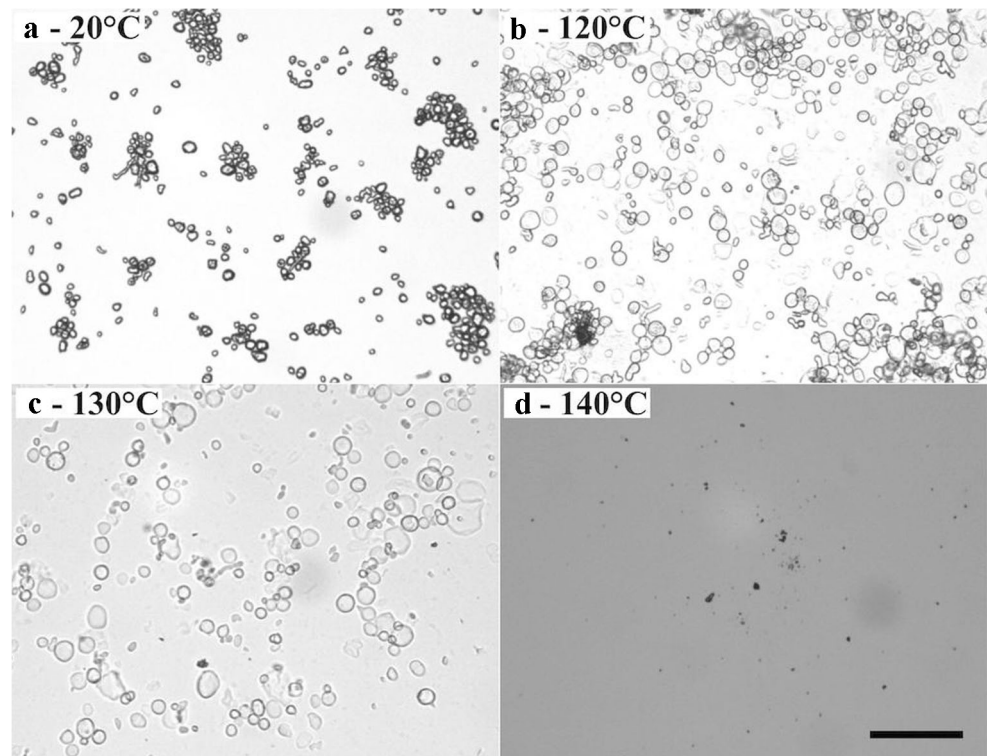
Starch pasting

The first step in the elaboration of starch aerogels is the formation of a starch gel. To this end, the starch is

Table 1 Specification of coaxial heat exchanger

Length	6 m
Coil internal diameter	260 mm
Number of turns	7
Internal tube inner diameter	15 mm
External tube outer diameter	24 mm
Tubes thickness	1 mm
Inner surface area	0.55 m ²

Fig. 4 Evolution of the amylo maize starch granule integrity for different pasting temperatures. **a** no pasting. **b** 120 °C. **c** 130 °C. **d** 140 °C. The scale bar represents 80 μm



dissolved in water at high temperature with an autoclave in a step called pasting.

The pasting temperature was varied for 1 wt.% pea and amylo maize starches slurry and pictures were taken after the pastings (Figs. 4 and 5). It can be observed

that the unprocessed pea starch granules are almost two times larger than the amylo maize ones, reminding that starch is a natural product which composition and shape vary with its origin. For temperature below 140 °C, no complete dissolution of the amylo maize starch was

Fig. 5 Evolution of the pea starch granule integrity for different pasting temperatures. **a** No pasting. **b** 105 °C. **c** 120 °C. **d** 130 °C. The scale bar represents 80 μm

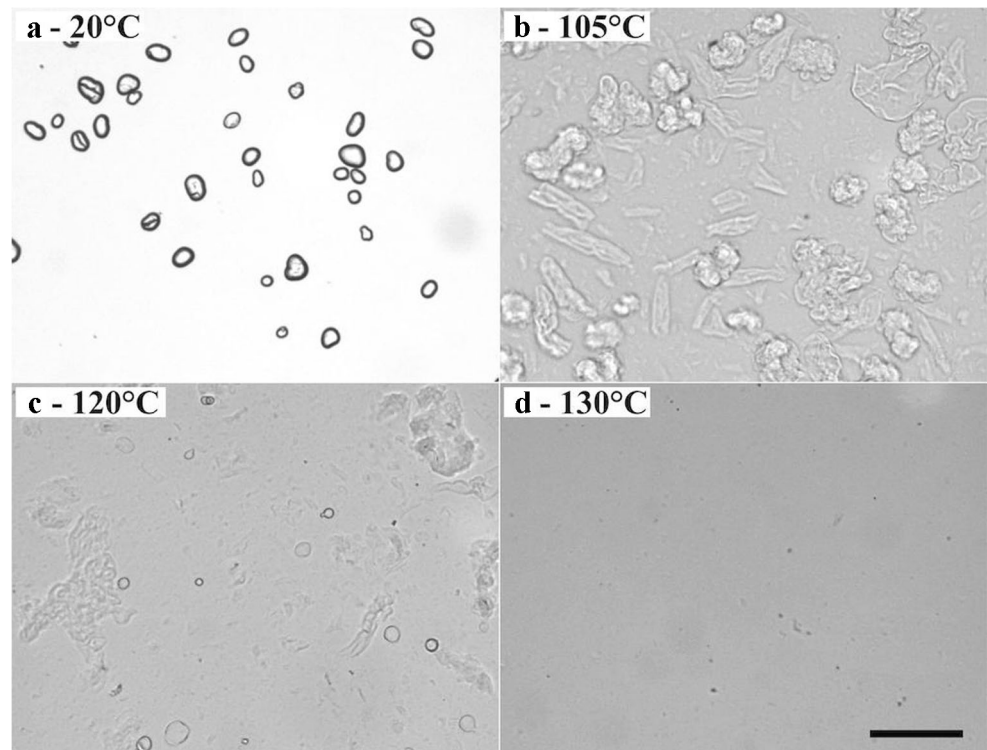
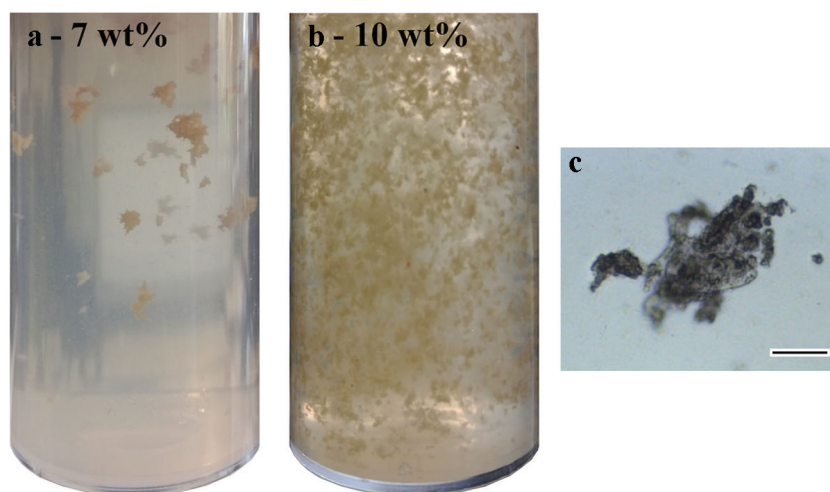


Fig. 6 Brown particles produced during the pasting of amylo maize starch, at 7 wt.% (a) and 10 wt.% (b) and under the microscope (c – scale bar is 10 μm)



possible, instead the granules swelled and retained their integrity (Fig. 4).

The pea starch granule presented intense swelling and lost their regular shape at 105 and 120 °C and their complete dissolution could be achieved at 130 °C.

Debet et al. [32] analysed the starch granule remanants (also known as ghost particles) and found out that they can be composed of up to 10 wt.% of amylose. This amylose fraction, trapped in the starch granule remanant, is not involved in the 3D gel network formation. This fact corresponds well with our experiments in which it was observed that starch gels containing ghost particles deformed easily, presenting a strong plastic behaviour compared to the elastic, fully pasted starch gels.

Pasting the amylo maize starch suspensions above 135 °C and for concentrations larger than 5 wt.% resulted in the formation of brown particles. These differed from the starch particle remanants (Fig. 4b and c) by their coloration but also by their aspect observed with the microscope (Fig. 6). Their presence and quantity varied as a function of the peak temperature reached during the pasting and also with the starch concentration. When the temperature was maintained under 135 °C and for concentrations of 5 wt.% and below, no brown particles were observed.

Hot filtration was used to concentrate some of these brown particles, and elemental analysis has been performed to determine their nitrogen content in comparison to that of the pure starch. We assumed that all the nitrogen came from proteins,

Table 2 Nitrogen and protein content of the pea and amylo maize starch and of the brown particle rich gel of amylo maize starch

Sample	Nitrogen content [wt.%]	Protein content [wt.%]
Particle rich material	0.5	3.1
Amylo maize starch	0.080	0.50
Pea starch	0.051	0.32

as neither starch nor eventual fatty acid contained in the starch granules have nitrogen in their structure. In accordance with the AOAC 2000 guidelines [33], the protein content was calculated by multiplying the nitrogen content by 6.25 (Table 2).

The brown particle rich material has a protein content (respectively nitrogen content) five times higher than the pure starch, demonstrating that the process by which they were formed, precipitated the protein rich material out of the bulk of the solution. This measurement and the temperature dependency for the brown particles formation supported the hypothesis that they were the product of Maillard reaction between the starch protein and the amylose or amylopectin during the pasting at temperature above 135 °C.

The pea starch has a lower protein content than the amylo maize, which could explain why it did not form such residues. Additionally, an older amylo maize batch from previous years did not produce such particles illustrating again the possible variability of the starch composition depending on the harvest.

Even though no apparent decrease in textural properties were observed when brown particles were not removed (data not included), the production of a precipitate in the initial

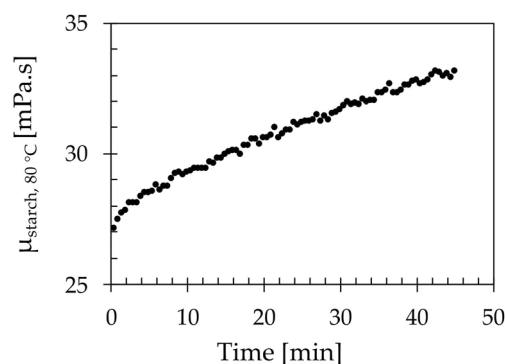


Fig. 7 Evolution of the shear viscosity of an amylo maize starch paste (10 wt.%) at a constant temperature (80 °C) and constant shear rate (1000 s^{-1})

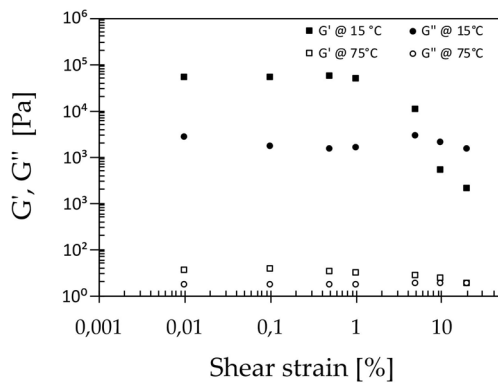


Fig. 8 Determination of the linear viscoelastic region (LVR) of two amylo maize system (10 wt.%), at 15 °C (gel) and 75 °C (paste) with a shear strain sweep done at 1 Hz

mixture is not desirable: it can be a source of fouling and can interfere with the emulsification process. This illustrates the importance of the initial starch characterization (in particular, for nitrogen content) to validate its compatibility with the pasting process. It also illustrates the possible effect of hot spots in the pasting device, which should be avoided by suitable operative measures.

Gelation temperature

Once the starch is fully dissolved in water after pasting, the gelation is triggered by reducing the temperature. Characterizing the gelation behaviour is critical to implement it into the particle production process. To this end, the starch pastes were studied with a rotational viscometer.

When the amylo maize starch paste viscosity was measured at constant temperature (80 °C) and constant shear rate (1000 s^{-1}), it was observed that the apparent shear viscosity continuously increased from 27 to 33 mPa.s in about 40 min as depicted on Fig. 7. This showed that even at 80 °C and under continuous shearing, there was a slow structure development (i.e. gelation) taking place.

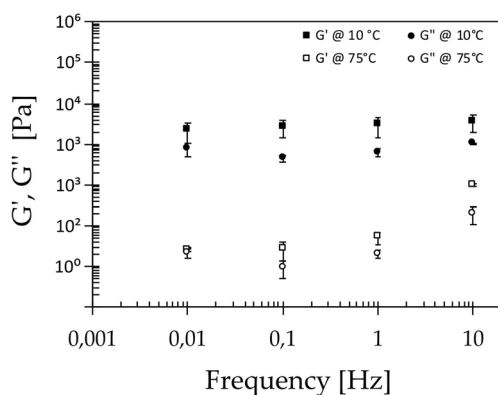


Fig. 9 Frequency sweep on two amylo maize systems (10 wt.%), at 10 °C (gel) and at 75 °C (paste) done with a shear strain of 0.1%

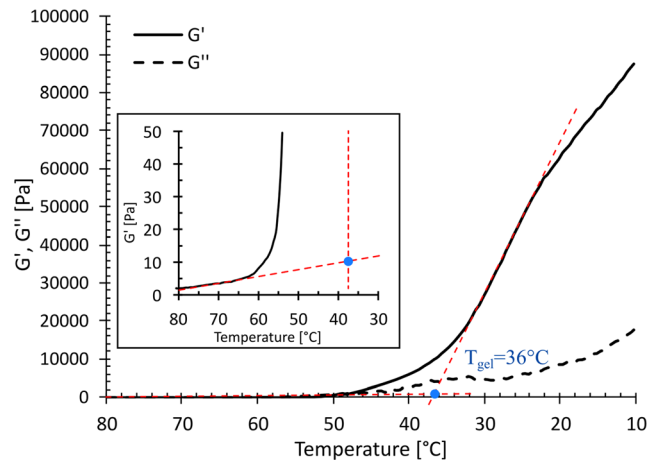


Fig. 10 Evolution of the elastic (G') and viscous moduli (G'') values during a temperature ramp from 80 to 10 °C (cooling rate 1 °C/min) for amylo maize starch paste (7 wt.%) as it transitioned from a liquid-like paste to a gel. The graph A in the inset corresponds to the magnified region around the gelation point with the two linear fits

Using the oscillation mode of the rheometer, a shear strain sweep was done at constant frequency (1 Hz) for a starch paste at 75 °C that behaved macroscopically like a liquid and for a starch gel at 15 °C (see Fig. 8). The elastic modulus (G') of the starch gel (at 15 °C) decreased strongly above a shear strain of 1%, delimiting the upper value of the linear viscoelastic region (LVR) in which oscillation can be used to characterized the gelation without damaging the gel structure. These first results were used to fix the shear strain to a value of 0.1% for the later experiments, allowing to record the elastic (G') and viscous moduli (G'') of the starch system as it transition from a paste to a gel.

For the starch gel at 15 °C, we observe that the elastic modulus is larger than the viscous modulus by a factor of about 100, characteristic of a solid-like material. It is interesting to observe that at 75 °C, when the starch paste behaves macroscopically like a liquid, the elastic modulus was already larger than the viscous modulus, with a G'/G'' ratio of about 1/2. This is characteristic of a weak gel structure and confirms the structure development in the starch paste observed during the measurement of the apparent viscosity at 80 °C shown in Fig. 7.

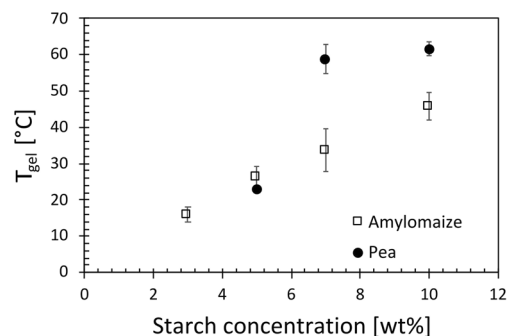


Fig. 11 Gelation temperature of pea and amylo maize starch paste at various concentrations

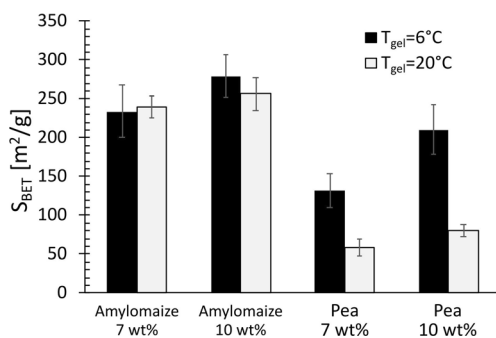


Fig. 12 Comparison of the specific surface area (S_{BET}) of amylo maize and pea starch aerogels for two gelation/retrogradation temperatures (6 and 20 °C) and two concentrations (7 and 10 wt.%)

These results demonstrated that once the temperature is decreased after the pasting, the starch paste is no longer stable and its rheological behaviour changes with time, even if the temperature is kept constant at 80–90 °C. This is of significant importance if the starch paste is to be processed with the emulsion gelation method, as the viscosity is critical to control the particle size distribution.

A frequency sweep was also done at a fixed shear strain of 0.1% for a gel at 10 °C and a paste at 75 °C (Fig. 9). As expected, the gel's G' and G'' displayed little sensitivity to the frequency, but the paste did behave like a liquid with increased G' and G'' at higher frequency [34].

The determination of the gelation temperature of the starch pastes was done by loading the pastes at 80 °C in the rheometer and recording the G' and G'' evolution (0.1% strain and 1 Hz frequency) with a cooling rate of 1 °C/min. Typical result of these experiments is shown in Fig. 10, where the elastic modulus increases in an accelerating manner with the decreasing temperature. Because G' was always above G'' , no cross-over point could be used to determine the gel point. Instead, two linear fits on the G' curve were done for the 80–70 °C and 37–22 °C temperature ranges (red dashed lines in Fig. 10), where the G' rate of changes were respectively the smallest ($-0.204 \text{ Pa}/^\circ\text{C}$) and the largest ($-3750 \text{ Pa}/^\circ\text{C}$). The gelation temperature was then determined by finding the intersection of the two linear fits (blue point in Fig. 10). The resulting

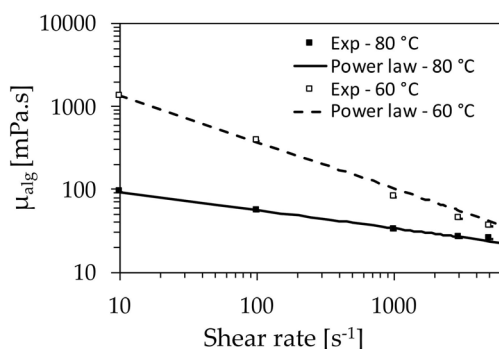


Fig. 13 Amylo maize starch paste (10 wt.%) viscosity measurement at 80 and 60 °C

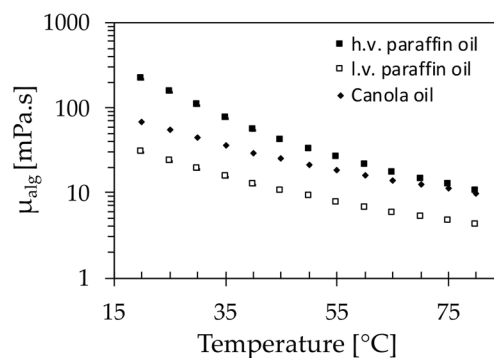


Fig. 14 Viscosities of the low-viscosity (l.v.) and high-viscosity (h.v.) paraffin oils and rapeseed oil at 15–80 °C measured at a shear rate of 1000 s^{-1}

gelation temperatures for pea and amylo maize starches (3 to 10 wt.% for) can be observed in Fig. 11.

For both starch types, as the concentration increased, the gelation temperature also increased. With the amylo maize starch, the increase was linear but for the pea starch a clear step can be observed between 5 and 7 wt.% and not much of a difference between 7 and 10 wt.%. This step gave the pea starch at 7 and 10 wt.% a significantly higher gelation temperature than the amylo maize starch.

Retrogradation and solvent exchange

Once the starch gels are formed, the gel network further developed with time during the so-called retrogradation step. We carried it at both 6 °C and at room temperature to evaluate how it influences the surface area (S_{BET}) of the final starch aerogels.

Suspensions of pea and amylo maize starch were pasted at 130 °C and 140 °C, respectively, poured into moulds and either allowed to gel and retrograde at room temperature or at 6 °C for 24 to 48 h. The gel monoliths were then solvent exchanged to reach ethanol concentrations from 95 to 99 wt.% and supercritically dried. No significant effect of the end concentration of ethanol in this range could be observed; their BET surface areas were thus averaged and plotted on Fig. 12.

For the amylo maize starch, no significant effect of the gelation temperature could be observed, making the gelation and retrogradation at lower temperature optional at such concentration. For the pea starch on the other hand, the effect of the gelation temperature was significant and the S_{BET} of the

Table 3 Parameters for the power law fit of the amylo maize starch paste (10 wt.%) apparent viscosity at 80 and 60 °C

Temperature [°C]	K	n
80	0.156	0.78
60	4.94	0.43

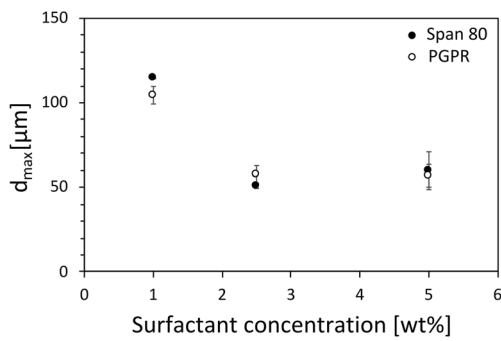


Fig. 15 Largest stable drop as a function of the surfactant concentration (Span80 – filled black circles and PGPR – empty circles) at 1050 RPM with the FBT

sample gelled at room temperature were half of the ones gelled at 6 °C.

Leloup et al. showed that the starch gel structure is composed of fibrils about 20 nm in diameter with a mesh size (distance between fibrils) of about 100 nm [35]. These fibrils are composed of amylose crystal presenting a characteristic B-type X-ray diffraction pattern corresponding to their double helix structure. Garcia-Gonzalez et al. observed the same characteristic X-ray diffraction pattern for starch aerogel [19] along with our results indicating a similar fibril structure in starch aerogel SEM pictures [36]. Lu et al. studied the retrogradation of potato amylose at different temperatures and showed that after 24 h, only 13% of amylose retrograded at 25 °C compared with 60% at 5 °C [37]. The temperature thus plays an important role in the formation of the crystalline structure of the starch gel which translates in the textural properties of resulting starch aerogels. The reason that such an effect was not observed for amylo maize

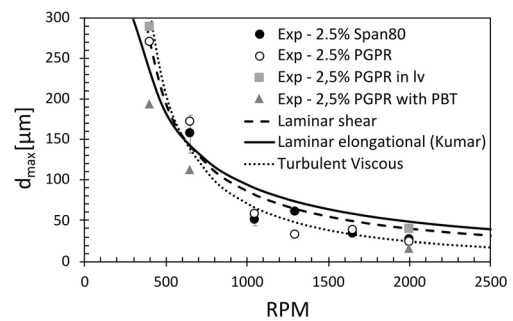


Fig. 17 Variation of the largest droplet size in the emulsion as a function of the stirring speed in the stirred vessel. Black circles correspond to 2.5 wt.% Span80 in high-viscosity paraffin oil with the FBT, white circles to 2.5 wt.% PGPR in high-viscosity paraffin oil with the FBT, grey triangles to 2.5 wt.% PGPR in high-viscosity paraffin oil with PBT and grey squares with 2.5 wt.% PGPR in low-viscosity oil with the FBT. The dashed line corresponds to the pure shear model with fitted IFT of 0.8 mN/m, the plain line represents the pure elongational model with fitted IFT of 19.9 mN/m and the dotted line – the turbulent viscous model with fitted IFT of 4.4 mN/m

starch could lie in the difference of amylose concentration between the two starches (66% vs. 45%).

For the same starch concentration, the amylo maize starch produced aerogel with higher surface area compared to the pea starch. The amylo maize starch has a significantly higher amylose content than the pea starch, which allows it to form aerogel with better textural properties as already discussed by Druel et al. [20].

Mehling et al. [14] obtained S_{BET} of 90 m²/g using high amylose corn starch Eurylon7 (similar to amylo maize used in this study) pasted at 95 °C and described a low mechanical stability. That can be attributed

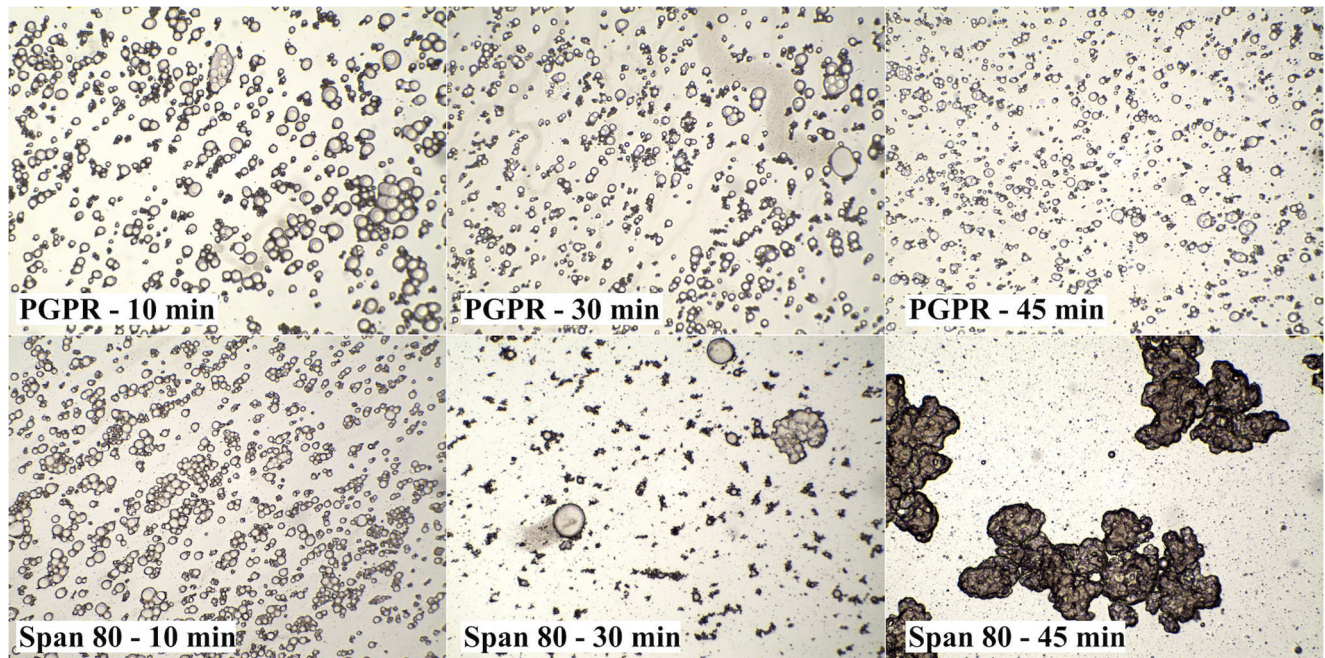


Fig. 16 Amylo maize starch gel microparticle suspensions produced by emulsion gelation in stirred tank with Span80 and PGPR for stirring time of 10, 30 and 45 min

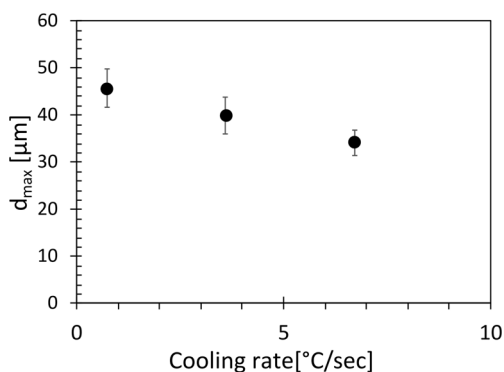


Fig. 18 Effect of the cooling rate during the gelation in emulsion on the gel microparticle diameter

to the incomplete pasting occurring at such temperatures, illustrating the importance of complete starch granule dissolution for the formation of strong starch gels and starch aerogels with good textural properties.

The pea and amylo maize starch aerogels produced in this study gave similar surface area as the one produced by Druel et al. [20] (respectively 221 m²/g and 254 m²/g from 8 wt.% starch suspensions) or by Garcia-Gonzalez et al. [19] (204–230 m²/g at 5–15 wt.%). However, Kenar's [21] starch-sodium palmitate complexes were having significantly higher surface area (362 m²/g at 5.5 wt.%).

Emulsion gelation

Viscosities of continuous and dispersed phases of an emulsion are critical parameters in the determination of the emulsion droplet size. The viscosity of the starch paste was measured at 80 and 60 °C (Fig. 13), and the viscosities of the different oils used for the emulsification (high- and low-viscosity paraffin oils and rapeseed oil) were measured in the 15–80 °C temperature range (Fig. 14).

The oils presented a Newtonian behaviour and no dependency on the shear rate could be observed. On the other hand, the starch paste demonstrated a strong shear thinning behaviour that is well described by a power law fit (Eq. 1); parameters can be found in Table 3.

$$\mu_{diss, app} = K\dot{\gamma}^{n-1} \quad (1)$$

Emulsifier type and concentration

The concentration of surfactant was varied during the emulsification from 1 to 5 wt.% for both PGPR and Span80. As depicted on Fig. 15, the effect of both surfactants was similar, with an effective particle size reduction as the concentration was increased from 1 to 2.5 wt.%. No further particle size

reduction was observed when increasing the surfactant concentration to 5 wt.%.

However, when the emulsification duration was increased, it was observed that the Span80 triggered an early gelation and agglomeration of the starch paste droplets when kept at 80 °C under stirring. Agglomerates begun to form after 30 min and the emulsion collapsed into large agglomerates after 45 min (Fig. 16). Ortega-Toro et al. reported amylose complexation with several Span surfactants (40, 60 and 80) [38] which matched our observations. PGPR did not exhibit such an effect and no agglomeration could be observed after 45 min (Fig. 16).

Thus, if the emulsification time is prolonged (e.g. emulsification in larger batches), the type of the surfactant used can be decisive. In our case, Span80 cannot be considered as a reliable surfactant for such cases.

Batch wise emulsification: stirred vessel

The stirring speed was varied from 400 to 2000 RPM with the FBT using both Span80 and PGPR at 2.5 wt.% in high-viscosity paraffin oil (black and white circles on Fig. 17). As the emulsification time was 10 min, no agglomeration was observed with the Span80, and the particle size obtained with the two surfactants was not significantly different. With the variation of stirring speed, the particle size could be controlled between 270 and 25 μm.

For these experiments, the impeller Reynolds number varied from 280 to 1450, corresponding to the transitional range between laminar and turbulent regime. Several expressions for the largest stable drop diameter in an emulsion are available in the literature. As we are neither fully laminar nor fully turbulent, three expressions corresponding to three different idealized flow types were evaluated:

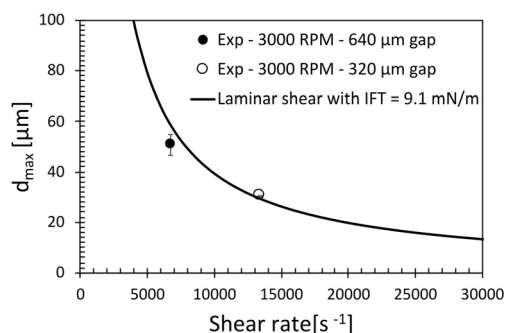


Fig. 19 Variation of the droplet size during the emulsification of the starch paste with the colloid mill as a function of the shear rate. The emulsification was done in high-viscosity paraffin oil with 2.5 wt.% PGPR. The black line represents the estimated largest droplet size in the emulsion obtained from the critical shear capillary number ($d_{max} = 2Ca_{crit}^e \sigma / \mu_{em} \dot{\gamma}$) with a fitted IFT of 9.1 mN/m

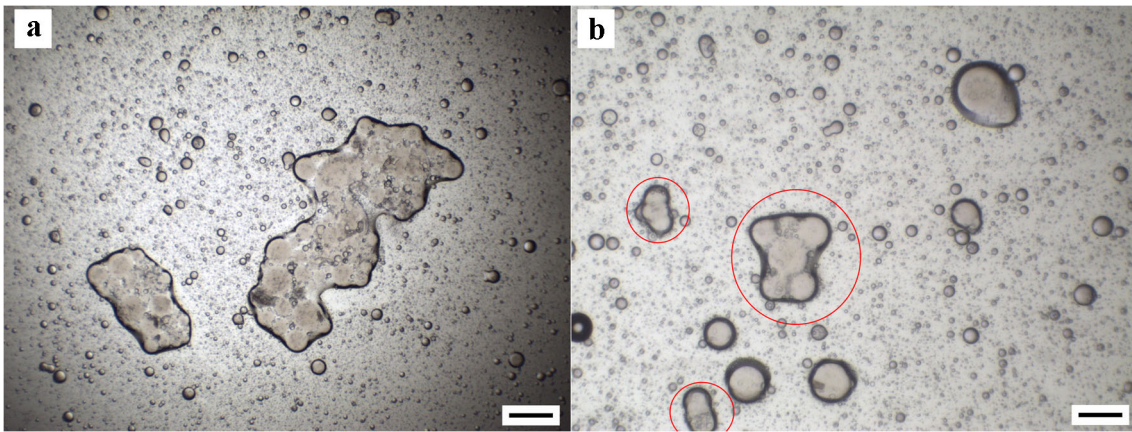


Fig. 20 Amylo maize starch (7 wt.%) gel microparticles produced with the emulsification carried out at 90 °C with 0.5 wt.% PGPR in rapeseed oil at 20 v% (heat exchanger outlet measured at 37 °C). The scale bars correspond to 200 μm for A and to 80 μm for B

- a. Laminar shear (Couette flow) with Eqs. 2 and 3 from de Bruijn [39]

$$d_{max}^s = \frac{2 Ca_{crit} \sigma}{\mu_{em} \dot{\gamma}} \quad (2)$$

$$\log_{10} Ca_{crit}^s = -0.506 - 0.0994 \log_{10} \lambda + 0.124 (\log_{10} \lambda)^2 - \frac{0.115}{\log_{10} \lambda - \log_{10} 4.08} \quad (3)$$

- b. Turbulent viscous with Eq. 4 from Kolmogorov [31]

$$d_{max,TV} = A_2 \epsilon_{max}^{-1/2} \mu_{cont}^{-1/2} \rho_{cont}^{-1/2} \sigma \quad (4)$$

- c. Laminar extensional (2D hyperbolic flow) with Eqs. 5 and from Hinch [40]

$$d_{max}^e = \frac{2 Ca_{crit}^e \sigma}{\mu_{em} \epsilon} \quad (5)$$

$$Ca_{crit}^e = \frac{0.15}{\lambda^{1/6}} \quad (6)$$

In Eqs. 3 and 6, λ refers to the viscosity ratio of the two emulsion's phase ($\lambda = \mu_{disp}/\mu_{cont}$), and ϵ_{max} in Eq. 4 is the maximal energy dissipation rate, which can be expressed according to Eq. 7 [41, 42].

$$\epsilon_{max} = \frac{P_{imp}}{V_{swept} \rho_{cont}} = \frac{Np N^5 D_{imp}^2}{(D_{imp}^2/4) h_{imp} \rho_{cont}} \quad (7)$$

If one assumes the droplet break-up to be controlled by a pure shear break-up model (a), the largest stable drop in emulsion can be estimated with Eq. 2 (dashed line in Fig. 17). The maximal shear rate, estimated using Bowen's equation [43] (Eq. 8), was used to calculate the apparent viscosity of the starch melt with the power law model parameters described in Table 3.

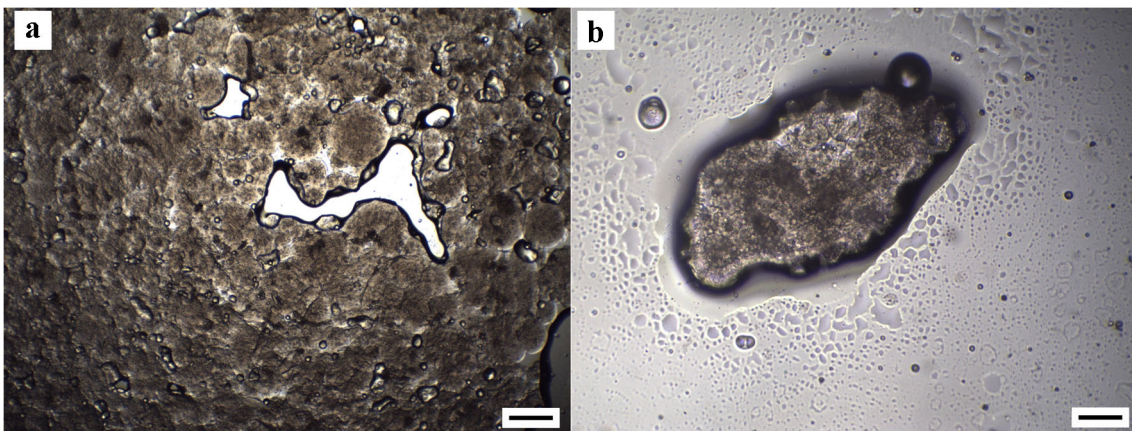


Fig. 21 Amylo maize starch (7 wt.%) gel microparticles produced with the emulsification carried out at 90 °C without surfactant in rapeseed oil at 20 v% (heat exchanger outlet measured at 35 °C). The scale bars correspond to 200 μm for both A and B

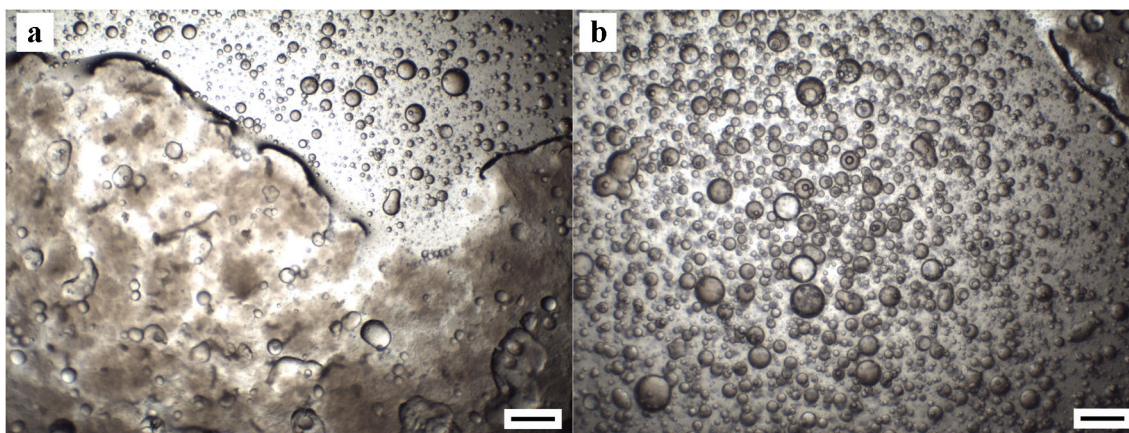


Fig. 22 Amylo maize starch (7 wt.%) gel microparticles produced with the emulsification carried out at 90 °C with 0.5 wt.% PGPR in rapeseed oil at 33 v% (heat exchanger outlet measured at 35 °C). The scale bars correspond to 200 μm for both A and B

$$\gamma_{\max} = 9.7N \left(\frac{d_{\text{imp}}}{d_{\text{tank}}} \right)^{0.3} \frac{d_{\text{imp}}}{W} \quad (8)$$

The shear critical capillary number was calculated with de Buijn equation (Eq. 3), considering the apparent viscosity of the starch melt for the dispersed phase and the viscosity of the emulsion calculated with the equation from Yaron and Gal-Or [44] (Eq. 9) to calculate the apparent viscosity ratio (Eq. 10).

$$\mu_{em} = \mu_{cont} \left(1 + \frac{5.5\Phi \left(4\Phi^{7/3} + 10 - \frac{84}{11}\Phi^{2/3} + \frac{4}{\lambda}(1-\Phi^{7/3}) \right)}{10(1-\Phi^{10/3}) - 25\Phi(1-\Phi^{4/3}) + \frac{10}{\lambda}(1-\Phi)(1-\Phi^{7/3})} \right) \quad (9)$$

$$\lambda_{app} = \frac{\mu_{disp,app}}{\mu_{em}} \quad (10)$$

The IFT was fitted to the experimental data and even though this approach provided a good description of the particle size, it required an IFT value of 0.8 mN/m. Such value is not realistic considering that the water-paraffin oil system has an IFT of 55 mN/m and that the water-paraffin-Span80 1 wt.%

oil system has an IFT of 2.3 mN/m after 2500 s at 20 °C [24]. Additionally, as it was discussed by Baudron et al. [24], the relevant IFT during the emulsification is larger than the measured equilibrium IFT values, further discrediting such small fitted IFT. With such considerations, we concluded that the droplet break-up did not occur only from a pure shear flow, which is expected in a stirred vessel with such Reynolds number. Nonetheless, Baudron et al. [24] showed that this approach yields better results for the emulsification of alginate solutions in paraffin oils at room temperature and with lower Reynolds number.

Even though the flow regime is not fully turbulent, the turbulent viscous model of Kolmogorov (b) was tested (dotted line in Fig. 17) to continue the investigation on the droplet break-up mechanism. It yielded a reasonable fit and description of the experimental data with an IFT value of 4.4 mN/m. To further confirm such description, further experiments with a PBT (represented as grey triangles on Fig. 17) were carried out, and smaller particles were produced at the same stirring rate. Additionally the oil viscosity was varied (represented as grey squares on Fig. 17), and only little effect on the particle size could be observed.

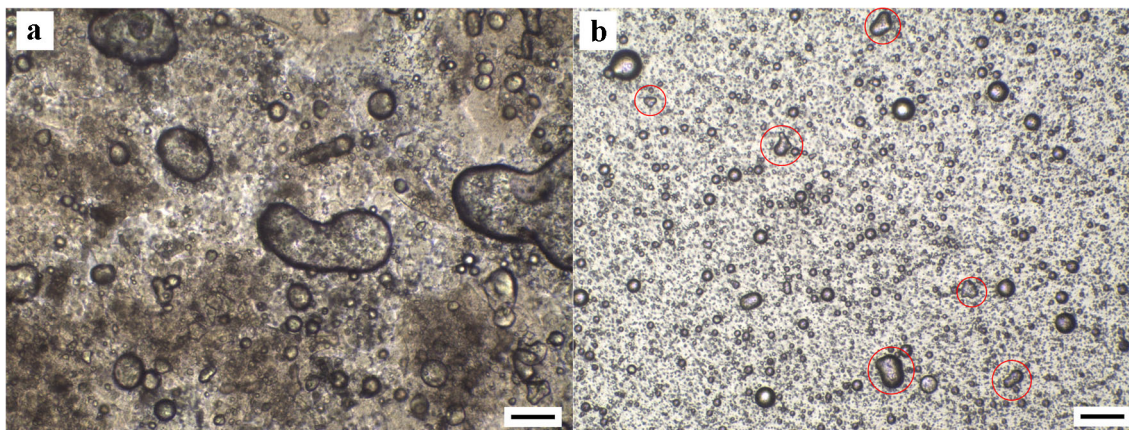


Fig. 23 Worst-case scenario – gelation without cooling (amylo maize starch 7 wt.%). The scale bars correspond to 200 μm for A and 80 μm for B

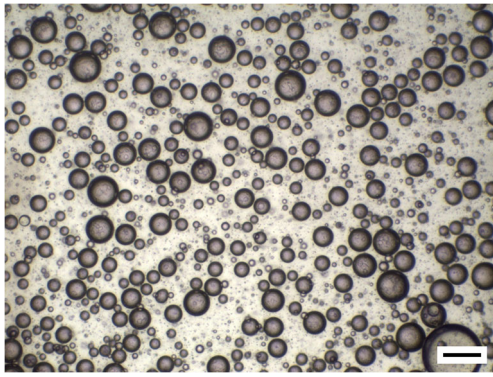


Fig. 24 Amylo maize starch (7 wt.%) gel microparticles produced with the emulsification carried out at 80 °C with 0.5 wt.% PGPR surfactant in rapeseed oil at 20 v% (heat exchanger outlet measured to be 32 °C). The scale bar corresponds to 80 μm

The FBT has a higher power number than the PBT [45] resulting in higher energy dissipation rate at the same stirring speed. If the break-up occurred in the turbulent viscous regime, the FBT should result in smaller particle size but the opposite is observed experimentally. Similarly, the model forecasts larger particle size with a lower continuous phase viscosity, but again no such effect was observed. These two supplementary sets of experiments confirmed that the droplet break-up cannot be represented properly with the turbulent viscous model.

Wille et al. [46] described the effect of macroscopic elongational flow on the emulsification in stirred tank. They showed that axial flow impellers yielded smaller droplets than their radial counterparts. With particle image velocimetry (PIV), they also observed larger macroscopic elongational flow produced by the axial flow impeller and concluded that this flow type played a crucial role in the droplet break-up. Such results matched well our observations and hinted that the droplet break-up in our system seemed to be more influenced by the elongational flow produced by the impeller.

Kumar et al. [47] proposed an approach to estimate the elongational rate in the vicinity of a radial flow impeller and

used it to describe the droplet break-up in elongational flows. Using their expression for the average elongational rate in the hyperbolic flow produced in the vicinity of the impeller (Eq. 11, with $\bar{f} = 7.8$) and the expression of the elongational critical capillary number Ca_{crit}^e proposed by Hinch [40] (Eq. 5), the size of largest stable drop in such flow field was estimated (plain line in Fig. 17) with a fitted IFT value of 19.9 mN/m.

$$\dot{\epsilon} = 6\pi N \bar{f} \quad (11)$$

This approach provides a good description of the droplet break-up with a reasonable IFT value, but the estimation is, however, not perfect, and a clear overestimation of the droplet size can be observed at higher stirring speeds. This is expected from the simplistic approach used to estimate the elongational rate but could be improved with PIV measurement or CFD simulation.

The flow in a stirred vessel is complex and heterogeneous, especially with a viscous continuous phase. We demonstrated that using models that only considers pure flow type (pure shear, pure elongational or turbulent) did not allow for a fully quantitative description of the droplet break-up in our system. We demonstrated in a previous work (Baudron et al. [24]) that the pure shear approach from de Bruijn could yield a good description of the emulsification in a similar set-up but operating at lower Reynolds number. This is consistent with the laminar flow assumption of this model that was not fully fulfilled in the present work. The elongational component of the flow seems to play the most important role in these flow conditions which the turbulent break-up approach could not properly represent.

In order to increase the production rate of starch gel particles, a semi-continuous approach can also be considered. The use of a colloid mill allows for the processing of the starch melt emulsion in a semi-continuous mode, i.e. to process larger quantities without changing the geometry of the emulsification device.

Batch wise gelation in emulsion: stirred vessel

To investigate the effect of the cooling rate on the particle size distribution during the batch emulsification, three cooling rates were investigated: Three emulsifications were carried out (FBT at 1050 PRM in high-viscosity paraffin oil with 2.5 wt.% PGPR) and cooled down to 20 °C while maintaining stirring (400 RPM) with a water bath at 6 °C, a water bath at 20 °C and in air at 20 °C, resulting in cooling rates of 6.7, 4.6 and 0.7 °C/s, respectively.

The particle sizes of the suspensions produced from the cooling of these three emulsions are displayed in Fig. 18. A significant effect of the cooling rate can be observed on the

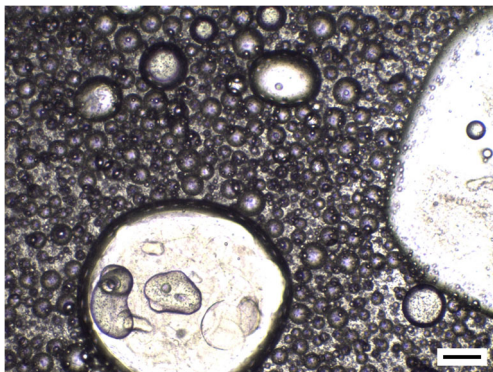
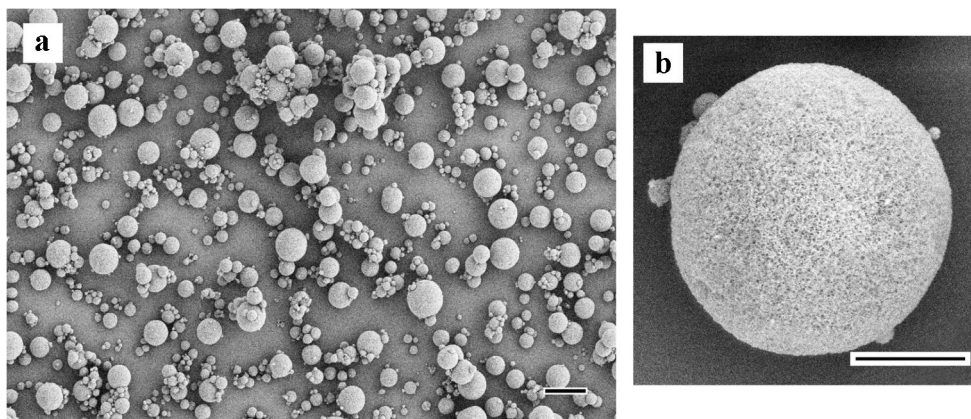


Fig. 25 Pea starch gel microparticles produced with the emulsification carried out at 90 °C with 0.5 wt.% PGPR in rapeseed oil at 50 v% (heat exchanger outlet measured at 35 °C). The scale bar corresponds to 80 μm

Fig. 26 Amylomaize starch aerogel (7 wt.%) microparticles produced with the emulsion gelation method. The scale bars correspond to 40 μm for A and 10 μm for B



final particle size, demonstrating that even with surfactant, some coalescence events can occur during slower gelations.

Semi-continuous emulsification: colloid mill

Colloid mills are emulsification devices commonly used in the industry for the processing of viscous systems. We investigated the emulsification of the starch paste in such a device for two shear rates by keeping the stirring speed constant at 3000 RPM and varying the gap between the rotor and the stator from 640 to 320 μm . In only one pass, particles with d_{max} between 30 and 50 μm were produced as represented in Fig. 19.

The Reynolds number in colloid mills can be calculated according to Eq. 12 [48] and was between 19 and 36 for this system, characterizing a laminar flow [49].

$$Re_{CM} = \frac{\rho \omega r_i \delta}{\mu_{em}} \quad (12)$$

where δ is the gap in the colloid mill. We used the pure shear critical capillary number from de Bruijn (Eq. 2), similarly to what was done previously for the stirred vessel to estimate the largest stable drop in the emulsion (plain line in Fig. 19), and used Eq. 13 for the shear rate estimation.

$$\dot{\gamma} = \frac{\pi d \omega}{\delta} \quad (13)$$

The pure shear model described well the experimental values, and a reasonable fitted IFT value of 9.1 mN/m was obtained. In this case, the laminar regime determined by the Reynolds number and the flow dominated by shear made this simple model a reliable description of the droplet break-up.

Semi-continuous gelation in emulsion: heat exchanger (HE)

In addition to the advantage the well-defined laminar regime, the colloid mill can be operated semi-continuously allowing the processing of larger quantities without changing the scale

of the emulsification device. Semi-continuous operation with the set-up depicted in Fig. 3 was realized, and gelation was achieved in-line in a coaxial heat exchanger.

As soon as the emulsion escapes the colloid mill, no further droplet break-up takes place because of the low shear in the piping, and as a result, the droplet size can increase through coalescence (ideally mitigated by the presence of surfactant). The colloid mill outlet also corresponds to the beginning of the emulsion cooling that trigger the gelation of the starch melt droplets. It is clear that once the starch droplets are gelled, no further coalescence can happen. Ideally, the droplets should gel as fast as possible in order to hinder coalescence and obtain the smallest gel particles possible.

The final particle size is influenced by the coalescence and gelation rate. To explore experimentally such a relationship, a reference experiment was carried out, and the resulting particles were compared with the ones from two experiments. The following parameters were varied in the latter experiments one after another:

- The surfactant and phase ratio were varied to influence the coalescence rate.
- The starch type, cooling or emulsification temperature was varied to influence the gelation rate.

The emulsification of amylo maize starch paste (7 wt.%) at 90 $^{\circ}\text{C}$ with 0.5 wt.% PGPR in rapeseed oil, with a phase ratio of 20 v% in a one pass through the colloid mill (3000 RPM – 636 μm gap), was chosen as the reference experiment. The emulsion was cooled in the heat exchanger and discharged in an unstirred vessel. At such conditions, large agglomerates, several hundreds of micrometres across, were produced (Fig. 20a) together with many round microparticles (Fig. 20b). The presence of agglomerates is the sign of partial coalescence and the result of an insufficient gelation rate. The temperature of the emulsion at the heat exchanger outlet was measured to be 37 $^{\circ}\text{C}$, which falls in the range of the gelation temperature for this system (34 \pm 5 $^{\circ}\text{C}$; see Fig. 10). This implies that the emulsion spend most of its residence time in

the heat exchanger above the gelation temperature and was thus prone to coalescence.

Effect of coalescence rate

The coalescence rate is influenced by the presence of surfactant and by the phase ratio. The surfactants reduce the coalescence probability in case of droplet collision, while a larger phase ratio increases the collision rate without affecting the coalescence probability.

An experiment without surfactant was performed and resulted in the formation of a gel block at the bottom of the receiving vessel (Fig. 21a) together with large agglomerates (Fig. 21b), but no spherical particle as it could be observed on Fig. 20 a when surfactants were used.

The formation of a gel block at the bottom of the receiving vessel could only have happened if at least a fraction of the droplets were not gelled at the HE outlet. The fact that this gel block was composed of seemingly agglomerated spherical particles (Fig. 21a) supports the hypothesis of a partial gelation. The HE outlet temperature measured to be 35 °C is in the range of gelation temperatures evaluated with the rheometer (34 ± 5 °C, Fig. 10). It is thus our first conclusion that the HE outlet temperature should be to some extent below the measured gelation temperature to ensure no coalescence. Additionally, these observations further demonstrate the effect of the surfactant in hindering the coalescence not only in the HE but also in the receiving vessel when the droplets (or partially gelled particles) sediments together at the bottom as no such gel block was produced in the reference experiment.

Carrying the emulsion gelation with 0.5 wt.% PGPR but at a higher phase ratio of 33 v% resulted in large agglomerates of several millimetres in size (Fig. 22a) but also yielded spherical particles (Fig. 22b) as opposed to the trial with no surfactant at lower phase ratio. Comparison of this result to the reference experiment illustrates the effect of a higher collision rate, resulting in a larger coalescence rate and thus producing larger agglomerates. Additionally, comparing this result with the surfactant free trial, we can prove that even with a higher collision rate (at a higher phase ratio), the presence of surfactant could hinder coalescence to a larger extent than simply lowering the collision rate.

Effect of cooling rate

The next experiment employed the same conditions as the reference one, but without cooling: the emulsion was passed through the HE but no cooling water was flowing. As no stirring was provided in the receiving vessel, most of the droplets coalesced at the bottom and yielded a gel block with oil inclusions (Fig. 23a). Only the small droplets that sedimented slow enough to gel before reaching the bottom of the vessel

resulted in gel microparticles (Fig. 23b). Even though slower gelation rates affect the final gel particle size (as demonstrated previously with the batch set-up), providing stirring in the receiving vessel can prevent the complete collapse of the emulsion. It is thus a critical part of the emulsion gelation set-up if the cooling capacity of the heat exchanger is not sufficient to reach the gelation temperature before the suspension is allowed to sediment in the receiving vessel.

As we could not vary the heat exchanger geometry or the cooling water temperature to accelerate the gelation rate, another experiment was performed in which the emulsification was carried out at a lower temperature of 80 °C. Indeed, by starting at a lower emulsification temperature, the gelation temperature should be reached faster with the given cooling capacity of the apparatus. This allowed to reduce the temperature of the emulsion at the heat exchanger outlet to 32 °C and produced spherical particles with no observable agglomerates (Fig. 24).

It is to be noted that the particle produced at 80 °C (Fig. 24) is larger than the one produced at 90 °C (Fig. 20) because of the significantly larger viscosity of the starch paste at 80 °C (see Fig. 13). If one would like to obtain smaller particles and avoid excessive coalescence, the rotation speed of the colloid mill should be increased in order to provide larger shear rate.

As discussed earlier, pea starch melts at 10 wt.% presented a significantly higher gelation temperature compared to the amylo maize at 7 wt.% (58 vs. 35 °C). This effect was exploited to further illustrate the gelation rate effect, and the emulsion of this starch melts was carried out at 90 °C, with 0.5 wt.% PGPR and with a phase ratio of 50 v%. These conditions did not result in the formation of any agglomerate even though the large particles observed on Fig. 25 indicate some degree of coalescence. Such coalescence events are not surprising at such large phase ratio, and these conditions are in no way optimal for proper particle production but are of strong interest for the understanding of the process. Indeed, this experiment demonstrates that a high gelation rate can certainly limit coalescence even in a system where the coalescence rate is expected to be high because of the large phase ratio.

Additionally, the large particles observed in Fig. 25 are a clear sign of coalescence, but the HE outlet temperature (35 °C), well below the system gelation temperature for this system (58 °C), eliminates the possibility to have any coalescence happening in the receiving vessel. The spherical nature of these large particles contrasts with the rough partial coalescence observed in the previous cases (Figs. 20a and b and 22a). This seems to indicate that the coalescence in the heat exchanger would yield large but round particles, while coalescence via sedimentation in the receiving vessel would be at the origin of the rough agglomerate. This observation also applies to the experiments with a lower emulsification temperature (Fig. 24), in which the HE outlet temperature seemed to have been low enough to avoid sedimentation

induced coalescence and in which the emulsion condition (surfactant and phase ratio) also inhibited coalescence in the HE.

These examples clearly demonstrate that an optimum in gelation and coalescence rates should be reached in order to allow for spherical gel microparticles production without the formation of agglomerates. The use of surfactant is critical for the coalescence control in our set-up as it was not possible to trigger the gelation fast enough before coalescence. Carrying the emulsification at lower temperatures did reduce the agglomerate production by allowing a quicker gelation and using pea starch that gels at higher temperature also proved to reduce the effect of coalescence.

Separation and supercritical drying

The gel particles were separated from the oil by sedimentation or centrifugation after the addition of a heavier aqueous phase, consisting of 70 wt.% water and 30 wt.% ethanol. The addition of ethanol was found to help the particle to transition more efficiently to the aqueous phase (compared to water only), and most of the particles were recovered. Additionally to helping the gel particles transition from the oil to the water phase, the addition of ethanol also allows to start the solvent exchange of the particles. It was then continued with fresh ethanol until the concentration was compatible with the supercritical drying (> 95 wt.%). Finally, the amylo maize starch gel (7 wt.%) microparticles (present as a slurry in ethanol) were supercritically dried. The resulting aerogel particles are shown in Fig. 26. They had BET surface area of $278 \pm 10 \text{ m}^2/\text{g}$. This value falls in the same range as the results obtained for the monolith presented in Fig. 12, demonstrating that the emulsion gelation process did not influence the final textural properties of the aerogel, allowing, however, its efficient shaping.

Conclusion

Two emulsion gelation processes for production of starch-derived aerogel microparticles were suggested: a batch and semi-continuous process. The formation of starch gels was investigated for two starch types – amylo maize and pea. We showed that amylo maize starch suspensions required higher temperature than pea starch to reach complete dissolution into water. Such a high temperature caused formation of brown particles with the amylo maize starch (possible Maillard reaction).

Using oscillatory rheometry, gelation in starch pastes was investigated. Higher starch concentration resulted in quicker gelation (higher gelation temperature), and above 5 wt.% pea starch pastes gelled significantly faster than their amylo maize counterparts.

The gelation and retrogradation temperature of the starch pastes were varied, and no significant effect could be observed on the specific surface area of amylo maize starch aerogel. On the other hand, pea starch aerogels produced with gelation and retrogradation carried out at 6 °C resulted in a specific surface area almost twice as large as the samples processed at 20 °C.

The emulsion gelation was investigated in a batch set-up (stirred vessel), and we showed that the description of the droplet size could neither succeed by considering pure Couette flow (pure shear) nor by using a turbulent viscous model. It appeared that the droplet break-up occurred in the elongational flow produced in the vessel which explained why the pitched blade turbine (axial flow impeller) produced smaller droplets than a flat blade turbine (radial flow impeller).

Additionally, the effect of the surfactant type on the process was demonstrated: Span80 and PGPR were used as surfactants in paraffin oil, and no difference could be observed in term of particle size until an emulsification time of 10 min. Above this time, the Span80 triggered the gelation and agglomeration of the starch paste droplets resulting in a complete phase separation.

The emulsion gelation of starch pastes was investigated for the first time in a semi-continuous set-up in which the emulsification was performed in a colloid mill. The well-defined Couette flow (pure shear) in such an apparatus allowed the description of the droplet break-up using a critical capillary number from the literature. A counter-current coaxial coiled heat exchanger was used to cool down the emulsion and trigger the gelation of the starch paste droplets demonstrating for the first time a semi-continuous emulsion gelation set-up.

Finally, the starch gel microparticles were supercritically dried, and their specific surface area was not significantly affected by the emulsion gelation method when compared with corresponding monoliths.

Therefore, we suggest to use the emulsion gelation process to produce starch aerogel microparticles in a (semi) continuous way. We hope that the process reported here will enable a broader application of starch aerogels in the life science.

Acknowledgements We are truly thankful to all the students who assisted carrying out the lab work, to Nestlé Product Technology Centre York for the financial support and to Dr. Olaf Häusler from Roquette Frère® for making the starch available to us and for the enlightening discussion.

Funding Information Open Access funding provided by Projekt DEAL.

Compliance with ethical standards

Conflict of interest The authors declare that they have no conflict of interest.

Open Access This article is licensed under a Creative Commons Attribution 4.0 International License, which permits use, sharing, adaptation, distribution and reproduction in any medium or format, as long as

you give appropriate credit to the original author(s) and the source, provide a link to the Creative Commons licence, and indicate if changes were made. The images or other third party material in this article are included in the article's Creative Commons licence, unless indicated otherwise in a credit line to the material. If material is not included in the article's Creative Commons licence and your intended use is not permitted by statutory regulation or exceeds the permitted use, you will need to obtain permission directly from the copyright holder. To view a copy of this licence, visit <http://creativecommons.org/licenses/by/4.0/>.

References

- Chidambareswarapattar C, Larimore Z, Sotiriou-Leventis C, Leventis N (2012) Mechanically strong nanoporous polyimides (aerogels) from anhydrides and isocyanates: A structure-property study, in: Abstr. Pap. Am. Chem. Soc., AMER CHEMICAL SOC 1155 16TH ST, NW, WASHINGTON, DC 20036 USA
- Rigacci A, Marechal JC, Repoux M, Moreno M, Achard P (2004) Preparation of polyurethane-based aerogels and xerogels for thermal superinsulation. *J Non-Cryst Solids* 350:372–378. <https://doi.org/10.1016/j.jnoncrysol.2004.06.049>
- Lee JK, Gould GL, Rhine W (2009) Polyurea based aerogel for a high performance thermal insulation material. *J Sol-Gel Sci Technol* 49:209–220. <https://doi.org/10.1007/s10971-008-1861-6>
- Chidambareswarapattar C, Xu L, Sotiriou-Leventis C, Leventis N (2013) Robust monolithic multiscale nanoporous polyimides and conversion to isomorphous carbons. *RSC Adv* 3:26459. <https://doi.org/10.1039/c3ra43717e>
- Nguyen ST, Feng J, Ng SK, Wong JPW, Tan VBC, Duong HM (2014) Advanced thermal insulation and absorption properties of recycled cellulose aerogels. *Colloids Surf Physicochem Eng Asp* 445:128–134. <https://doi.org/10.1016/j.colsurfa.2014.01.015>
- Fischer F, Rigacci A, Pirard R, Berthon-Fabry S, Achard P (2006) Cellulose-based aerogels. *Polymer* 47:7636–7645. <https://doi.org/10.1016/j.polymer.2006.09.004>
- Demilecamps A, Beauger C, Hildenbrand C, Rigacci A, Budtova T (2015) Cellulose–silica aerogels. *Carbohydr Polym* 122:293–300. <https://doi.org/10.1016/j.carbpol.2015.01.022>
- Rudaz C, Courson R, Bonnet L, Calas-Etienne S, Sallée H, Budtova T (2014) Aeropectin: fully biomass-based mechanically strong and thermal superinsulating aerogel. *Biomacromolecules* 15:2188–2195. <https://doi.org/10.1021/bm500345u>
- Rudaz C (2013) Cellulose and pectin aerogels: towards their nano-structuration, MINES ParisTech
- Tkalec G, Knez Ž, Novak Z (2015) Fast production of high-methoxyl pectin aerogels for enhancing the bioavailability of low-soluble drugs. *J Supercrit Fluids* 106:16–22. <https://doi.org/10.1016/j.supflu.2015.06.009>
- Quraishi S, Martins M, Barros AA, Gurikov P, Raman SP, Smirnova I, Duarte ARC, Reis RL (2015) Novel non-cytotoxic alginate–lignin hybrid aerogels as scaffolds for tissue engineering. *J Supercrit Fluids* 105:1–8. <https://doi.org/10.1016/j.supflu.2014.12.026>
- Escudero RR, Robitzer M, Di Renzo F, Quignard F (2009) Alginate aerogels as adsorbents of polar molecules from liquid hydrocarbons: hexanol as probe molecule. *Carbohydr Polym* 75:52–57. <https://doi.org/10.1016/j.carbpol.2008.06.008>
- Mallepally RR, Bernard I, Marin MA, Ward KR, McHugh MA (2013) Superabsorbent alginate aerogels. *J Supercrit Fluids* 79:202–208. <https://doi.org/10.1016/j.supflu.2012.11.024>
- Mehling T, Smirnova I, Guenther U, Neubert RHH (2009) Polysaccharide-based aerogels as drug carriers. *J Non-Cryst Solids* 355:2472–2479. <https://doi.org/10.1016/j.jnoncrysol.2009.08.038>
- Marco ID, Baldino L, Cardea S, Reverchon E (2015) Supercritical gel drying for the production of starch aerogels for delivery systems. *Chem Eng Trans*:307–312. <https://doi.org/10.33031/CET1543052>
- Ubeyitogullari A, Ciftci ON (2016) Formation of nanoporous aerogels from wheat starch. *Carbohydr Polym* 147:125–132. <https://doi.org/10.1016/j.carbpol.2016.03.086>
- De Marco I, Reverchon E (2017) Starch aerogel loaded with poorly water-soluble vitamins through supercritical CO₂ adsorption. *Chem Eng Res Des* 119:221–230. <https://doi.org/10.1016/j.cherd.2017.01.024>
- Goimil L, Braga MEM, Dias AMA, Gómez-Amoza JL, Concheiro A, Alvarez-Lorenzo C, de Sousa HC, García-González CA (2017) Supercritical processing of starch aerogels and aerogel-loaded poly(ϵ -caprolactone) scaffolds for sustained release of ketoprofen for bone regeneration. *J CO₂ Util* 18:237–249. <https://doi.org/10.1016/j.jcou.2017.01.028>
- García-González CA, Smirnova I (2013) Use of supercritical fluid technology for the production of tailor-made aerogel particles for delivery systems. *J Supercrit Fluids* 79:152–158. <https://doi.org/10.1016/j.supflu.2013.03.001>
- Druel L, Bardl R, Vorwerg W, Budtova T (2017) Starch aerogels: a member of the family of thermal superinsulating materials. *Biomacromolecules* 18:4232–4239
- Kenar JA, Eller FJ, Felker FC, Jackson A, Fanta GF (2014) Starch aerogel beads obtained from inclusion complexes prepared from high amylose starch and sodium palmitate. *Green Chem*:1921–1930. <https://doi.org/10.1039/c3gc41895b>
- Ching SH, Bansal N, Bhandari B (2017) Alginate gel particles—a review of production techniques and physical properties. *Crit Rev Food Sci Nutr* 57:1133–1152. <https://doi.org/10.1080/10408398.2014.965773>
- Ganesan K, Budtova T, Ratke L, Gurikov P, Baudron V, Preibisch I, Niemeyer P, Smirnova I, Milow B (2018) Review on the production of polysaccharide aerogel particles. *Materials* 11:2144. <https://doi.org/10.3390/ma11112144>
- Baudron V, Gurikov P, Smirnova I (2019) A continuous approach to the emulsion gelation method for the production of aerogel micro-particle. *Colloids Surf Physicochem Eng Asp* 566:58–69. <https://doi.org/10.1016/j.colsurfa.2018.12.055>
- Kleemann C, Selmer I, Smirnova I, Kulozik U (2018) Tailor made protein based aerogel particles from egg white protein, whey protein isolate and sodium caseinate: influence of the preceding hydrogel characteristics. *Food Hydrocoll* 83:365–374. <https://doi.org/10.1016/j.foodhyd.2018.05.021>
- García-González CA, Jin M, Gerth J, Alvarez-Lorenzo C, Smirnova I (2015) Polysaccharide-based aerogel microspheres for oral drug delivery. *Carbohydr Polym* 117:797–806. <https://doi.org/10.1016/j.carbpol.2014.10.045>
- Alnaief M, Alzaitoun MA, García-González CA, Smirnova I (2011) Preparation of biodegradable nanoporous microspherical aerogel based on alginate. *Carbohydr Polym* 84:1011–1018. <https://doi.org/10.1016/j.carbpol.2010.12.060>
- Wang X, Wang X, Liu L, Bai L, An H, Zheng L, Yi L (2011) Preparation and characterization of carbon aerogel microspheres by an inverse emulsion polymerization. *J Non-Cryst Solids* 357:793–797. <https://doi.org/10.1016/j.jnoncrysol.2010.11.015>
- Gu S, Zhai C, Jana SC (2016) Aerogel microparticles from oil-in-oil emulsion systems. *Langmuir* 32:5637–5645. <https://doi.org/10.1021/acs.langmuir.6b01043>
- Alnaief M, Smirnova I (2011) In situ production of spherical aerogel microparticles. *J Supercrit Fluids* 55:1118–1123. <https://doi.org/10.1016/j.supflu.2010.10.006>

31. Vankova N, Tcholakova S, Denkov ND, Ivanov IB, Vulchev VD, Danner T (2007) Emulsification in turbulent flow. *J Colloid Interface Sci* 312:363–380. <https://doi.org/10.1016/j.jcis.2007.03.059>
32. Debet MR, Gidley MJ (2007) Why do gelatinized starch granules not dissolve completely? Roles for amylose, protein, and lipid in granule “ghost” integrity. *J Agric Food Chem* 55:4752–4760. <https://doi.org/10.1021/jf070004o>
33. Association of Official Analytical Chemists, Horwitz W, eds., *Food composition, additives, natural contaminants*, 17th, AOAC International, Arlington, 2000
34. Rao MA (2014) *Rheology of fluid, semisolid, and solid foods*. Springer US, Boston. <https://doi.org/10.1007/978-1-4614-9230-6>
35. Leloup VM, Colonna P, Ring SG, Roberts K, Wells B (1992) Microstructure of amylose gels. *Carbohydr Polym* 18:189–197. [https://doi.org/10.1016/0144-8617\(92\)90063-V](https://doi.org/10.1016/0144-8617(92)90063-V)
36. Baudron V, Gurikov P, Smirnova I, Whitehouse S (2019) Porous Starch Materials via Supercritical- and Freeze- Drying, 14
37. Lu T, Jane J, Keeling PL (1997) Temperature effect on retrogradation rate and crystalline structure of amylose. *Carbohydr Polym* 33: 19–26
38. Ortega-toro R, Jiménez A, Talens P, Chiralt A (2014) Effect of the incorporation of surfactants on the physical properties of corn starch films. *Food Hydrocoll* 38:66–75. <https://doi.org/10.1016/j.foodhyd.2013.11.011>
39. Bruijn RRD (1989) Deformation and breakup of drops in simple shear flows. <https://doi.org/10.6100/ir318702>
40. Hinch EJ, Acrivos A (1979) Steady long slender droplets in two-dimensional straining motion. *J Fluid Mech* 91:401. <https://doi.org/10.1017/S0022112079000227>
41. Alopaeus V, Koskinen J, Keskinen KI, Majander J (2002) Simulation of the population balances for liquid–liquid systems in a nonideal stirred tank. Part 2—parameter fitting and the use of the multiblock model for dense dispersions. *Chem Eng Sci*. 57:1815–1825
42. Kumar S, Kumar R, Gandhi KS (1991) Alternative mechanisms of drop breakage in stirred vessels. *Chem Eng Sci* 46:2483–2489
43. Bowen R (1986) Unraveling the mysteries of shear-sensitive mixing systems. *Chem Eng* 93:55–63
44. Yaron I, Gal-Or B (1972) On viscous flow and effective viscosity of concentrated suspensions and emulsions: effect of particle concentration and surfactant impurities. *Rheol Acta* 11:241–252. <https://doi.org/10.1007/BF01974767>
45. Paul EL, Atiemo-Obeng VA, Kresta SM (eds) (2004) *Handbook of industrial mixing: science and practice*. Wiley-Interscience, Hoboken
46. Wille BM, Langer G, Werner U (2001) The influence of macroscopic elongational flow on dispersion processes in agitated tanks. *Chem Eng Technol* 24:119–127
47. Kumar S, Ganvir V, Satyanand C, Kumar R, Gandhi KS (1998) Alternative mechanisms of drop breakup in stirred vessels. *Chem Eng Sci* 53:3269–3280
48. Maindarkar S, Dubbelboer A, Meuldijk J, Hoogland H, Henson M (2014) Prediction of emulsion drop size distributions in colloid mills. *Chem Eng Sci* 118:114–125. <https://doi.org/10.1016/j.ces.2014.07.032>
49. Noui-Mehidi MN, Ohmura N, Kataoka K (2005) Dynamics of the helical flow between rotating conical cylinders. *J Fluids Struct* 20: 331–344. <https://doi.org/10.1016/j.jfluidstructs.2004.12.001>

Publisher's note Springer Nature remains neutral with regard to jurisdictional claims in published maps and institutional affiliations.